Yttria-Stabilized Zirconia Aided Electrochemical Investigation on Ferric Ions in Mixed Molten Calcium and Sodium Chlorides

HONGBO HU,[1,2] YUNMING GAO,[1,2,*] YIGUI LAO,[1,2] QINGWEI QIN, [1,2]

GUANGQIANG LI, [1,2] and GEORGE Z. CHEN[1,2,3]

1. The State Key Laboratory of Refractories and Metallurgy, Wuhan University of Science and Technology, Wuhan 430081, China.
2. Key Laboratory for Ferrous Metallurgy and Resources Utilization of Ministry of Education, Wuhan University of Science and Technology, Wuhan 430081, China.
3. Department of Chemical and Environmental Engineering, and Energy Engineering Research Group, Faculty of Science Engineering, University of Nottingham Ningbo China, Ningbo 315100, China.

*Corresponding Author E-mail: gaoyunming@wust.edu.cn

ABSTRACT

Electrolytic reduction of dissolved iron oxide to metal iron in molten salts with an inert anode is an alternative short route for steelmaking without CO_2 emissions. A novel and simple integrated yttria-stabilized zirconia (YSZ) cell was constructed from a YSZ tube with a closed end. The YSZ tube played multiple functions, including the container for the molten salts, the solid electrolyte membrane in the O^{2-} | YSZ | Pt | O_2 (air) reference electrode (RE), and the solid electrolyte membrane between the working and counter electrodes (WE and CE). Electrochemical behavior of ferric ions (Fe^{3+}) that were formed by dissolution of 0.5 wt pct Fe_2O_3 in the molten $CaCl_2$-NaCl eutectic mixture was investigated on a Pt WE at 1273 K by various electrochemical techniques including cyclic voltammetry, linear scan voltammetry, square wave voltammetry, chronopotentiometry, chronoamperometry, and potentiostatic electrolysis. Analysis of the mechanism of electrode reactions was further assisted by scanning electron microscopy, energy dispersive X-ray spectroscopy, and X-ray diffraction. Some electrochemical parameters were obtained, including the number of exchanged electrons and the diffusion coefficient of ferric ions in the mixed molten salts. The results from various electrochemical techniques are in good agreement with each other, and show that the electrochemical reduction of Fe^{3+} to Fe in the molten salt mixture could be a single three-electron transfer step and diffusion controlled reaction that was also possibly reversible. This work may form the foundation for extraction of iron and alloys from molten salts and also provid a stable O^{2-} | YSZ | Pt | O_2 (air) RE with wide applicability for investigation on electrochemical properties of other electroactive metal oxides in molten salts.

KEY WORDS: electrochemical behavior; ferric ions; molten salt; electrodeposition; reference electrode; zirconia-based solid electrolyte

I. INTRODUCTION

The current industrial approach to iron and steel smelting is a multi-step, long and complex, and energy and emission intensive process. Firstly, the molten iron is produced from carbothermic reduction of iron ore in the blast furnace (ca. 1773 K), and then steel is derived from decarburization of the molten iron in the basic oxygen furnace (ca. 1873 K), followed by refining and alloying. Electrolytic reduction of iron compounds (mainly halides or oxides) in molten salt electrolyte using an inert oxygen-evolving anode is an alternative and short process for ironmaking without CO_2 emissions.[1-9] Aiming to drastically reduce CO_2 emissions, Europe has set up an ultra-low CO_2 steelmaking (ULCOS) program which includes electrolytic reduction in molten salts.[10,11] Molten oxide electrolysis (MOE, ca. 1873 K) was proposed for production of liquid iron in the United States.[12-16] Also, direct electrolytic reduction of solid iron oxide bulk in molten salts, *i.e.*, the Fray-Farthing-Chen (FFC) Cambridge process (ca. 1173 K), has also been extensively investigated in laboratory.[17-21] It is worth noting that molten salt electrolysis proceeds at much lower temperatures and hence should incur less heat loss than the other processes.

Since iron can be extracted from molten salts at medium temperatures, and Fe_2O_3 is a resourceful and low-cost raw material, electrolytic production of iron from Fe_2O_3 dissolved in molten salts has drawn increasing attention in recent years. Electrochemical behavior of Fe^{3+} ions in molten salts has been studied by some researchers and some findings have been obtained from these early studies.[6-9] However, it is difficult to draw an unambiguous conclusion from these early studies because different experimental conditions were applied, including molten salt composition, solute concentration, and temperature. In addition, the use of different working electrodes (WEs) and reference electrodes (REs) in the early studies also made it inconvenient to make systematic and comprehensive comparisons. Particularly, the reliability of potential values is still in doubt when measured against those pseudo-REs of metal wires in molten salts.[22,23]

Zirconia (ZrO_2) doped with magnesia (MgO), yttria (Y_2O_3), or the like is a kind of solid electrolyte (shorted as MSZ or YSZ, *etc*.) that is featured by high conductivity to O^{2-} ions, insignificant electronic conductivity, and good resistance to erosion by molten salts at high temperatures. These zirconia-based solid electrolytes are widely used in the metallurgical industry and fundamental research.[24-39] For example, they are used to help the determination of the activity[24,25] and diffusion coefficient [26,27] of oxygen in molten metals, and of the activity of FeO in molten slags,[28,29] to assist the electrolytic refining of molten metals,[30,31] and the extraction of metals from metal oxides dissolved in molten salts and slags.[32-36] Furthermore, in order to conduct electrochemical research on molten media containing O^{2-} ions, MSZ or YSZ can also be used to construct a stable RE, such as the "O^{2-} | MSZ (or YSZ) | Pt | O_2 (air)" RE at high temperatures.[37-39] Since the O_2 partial pressure is very stable in the air, either stationary or flowing, the O^{2-} | MSZ (or YSZ) | Pt | O_2 (air) RE is preferred for its good stability and reproducibility. However, this type of RE is seldom applied to the fundamental electrochemical analysis of molten salts to date.[40-42]

We recently utilized an MSZ tube to fabricate an integrated electrochemical cell with the O^{2-} | MSZ | Pt | O_2 (air) RE similar to the one used by Pal et al.,[38] which is simple and unique in structure and fabrication. With multiple functions such as the container for molten slags, and the electron insulating but ion conducting membrane to separate the anolyte and catholyte, the MSZ tube with a closed end was successfully applied to the electrochemical analyses in molten slags containing FeO or NiO at ultra-high temperatures.[43,44]

It is known that the O^{2-} ion conductivity of YSZ is usually higher than that of MSZ at the same temperature. Thus, it was thought that YSZ could offer a sufficiently high O^{2-} ion conductivity at temperatures lower than what is needed for MSZ to achieve the same conductivity. In this work, a YSZ tube with a closed end was used to build an integrated electrochemical cell with the "O^{2-} | YSZ | Pt | O_2 (air)" RE for a systematic investigation on the property of Fe^{3+} ions on a Pt WE in the molten $CaCl_2$-NaCl eutectic mixture [45] containing dissolved 0.5 wt pct Fe_2O_3 at 1273 K. The experimentally determined operating temperature range in this work was from 1173 K to 1373 K to enable sufficient oxide ion conductivity of the YSZ tube, and also to avoid significant evaporation of the molten salt and attack to the YSZ tube by the molten salt.

Various electrochemical techniques were applied, such as cyclic voltammetry/voltammogram (CV), linear scan voltammetry/voltammogram (LSV), square wave voltammetry/voltammogram (SWV), chronopotentiometry/chronopotentiogram (CP), chronoamperometry/chronoamperogram (CA), and potentiostatic electrolysis. Here, the $CaCl_2$-NaCl eutectic mixture was chosen as the medium in terms of source, cost, and wide application. Chen [46] and Haarberg et al. [47] studied the solubility of Fe_2O_3 in $CaCl_2$-NaCl melt, respectively. It can be reasonably assumed from their work that the solubility of Fe_2O_3 in the molten $CaCl_2$-NaCl eutectic mixture is above 1.5 wt pct at 1273 K and the Fe ions mainly exist in the +3 valence in the present work.

This work is part of an ongoing systematic research program aiming at developing a green electrolytic process for iron- and steelmaking without emission of CO_2. In the research, a YSZ tube with a closed end was employed as the container of the molten salts, and also as the ion conducting but electron insulating membrane to electronically and physically separate the WE and CE. The YSZ tube was attached with a Pt CE and an "O^{2-} | YSZ | Pt | O_2 (air)" RE (in fact an "O^{2-}|O_2" RE) on the external wall, forming a simple integrated electrochemical cell. In the work of Pal et al.,[32-34] the solid oxide membrane (SOM) was a tube with a closed end which was immersed in the molten salt and acted only as the ion conducting to electronically and physically separate the anode and cathode. Specifically, their SOM was not used to incorporate the RE. Consequently, the SOM cell of Pal et al. was mainly used for electrolysis for metal extraction, while the integrated cell is designed to enable various electrochemical analyses in high-temperature melts.

The goal of the current investigation is to demonstrate the use of the novel integrated cell as a simple and convenient tool for studying the electrochemical behavior of iron oxide dissolved in molten salts, while we hope that the findings reported in the work will benefit similar studies of

other high-temperature electrolytes and the future design of the industrial cell capable of continuous operation, and the selection, monitor, and control of the process variables for optimal production.

II. EXPERIMENTAL

A. *Preparation of Salt Specimen*

All chemical reagents used in this work were granules or powders of the analytical grade. In order to avoid proportioning deviation caused by moisture absorption, a dehydration test was first conducted at a chamber-type resistance furnace, in which the as-received powders of $CaCl_2$ and NaCl were heated to and held at 773 K for 5 hours and the moisture contents were estimated to be 3.4 and 1.05 wt pct, respectively, according to weight loss of the heated salts. When weighing a salt mixture with 65 wt pct $CaCl_2$ and 35 wt pct NaCl,[45] the moisture content was subtracted from the raw reagents. The Fe_2O_3 reagent was heated at 473 K for 2 hours in a vacuum-drying-oven with absolute pressure below 133 Pa. The dried Fe_2O_3 was added to the salt mixture of $CaCl_2$-NaCl to reach the composition of 0.5 wt pct Fe_2O_3. The mixed salts and oxide powders were subjected to ball milling in a sealed polyurethane jar with agate balls on a horizontal roller for 3 hours at 25 RPM to ensure uniform mixing. After milling and separation from the agate balls on a clean 8-mesh SS screener, the $CaCl_2$-NaCl-Fe_2O_3 mixture was ready for use, or stored in a desiccator for future purposes.

B. *Construction of Electrochemical Cell*

The integrated electrochemical cell was made from a YSZ (Y_2O_3, 8 mol pct) tube with one closed end and three electrodes, as schematically illustrated in Figure 1.
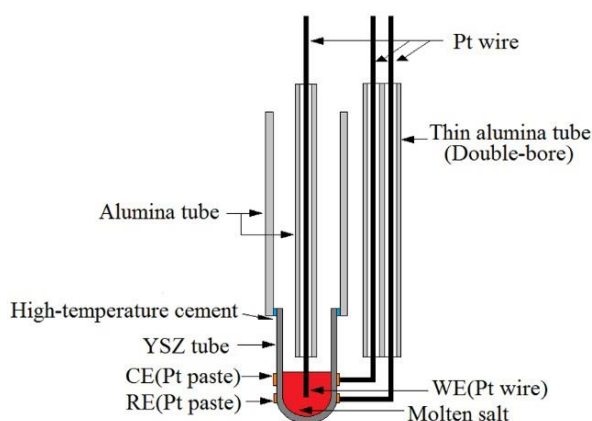
Fig. 1—Schematic illustration of the YSZ-based integrated three-electrode cell for electrochemical analyses in molten salts at high temperatures (1273 K in this work).

The YSZ tube was supplied by Tianchang Hainas instrument Co., Ltd., where the YSZ tube

5

180   was prepared by isostatic pressing finely synthetic YSZ powder and sintering, and where the

181   synthetic YSZ powder was also purchased from outside. The size of YSZ tube used was 6.7 and

182   9.6 mm in inner and outer diameter, respectively, and 100 mm in length. The Pt paste (supplied by

183   Sino-Platinum Metals Co., Ltd, China) was uniformly painted on two adjacent circular parts of the

184   outer surface of the YSZ tube near the closed end. The Pt paste-painted YSZ tube was then dried

185   in the air, followed by sintering in air for 30 minutes in the chamber-type resistance furnace at

186   1173 K. Thus, two circular electrodes with good adhesion to the YSZ tube could be obtained. The

187   circular Pt electrode near the bottom was the RE (area: 0.91 cm^2), and the other was the CE (area:

188   1.52 cm^2). A long Pt wire (purity: 99.95 pct; diameter: 0.5 mm) lead was fastened to the YSZ tube

189   with a thin Pt wire (diameter: 0.3 mm) at each of the two circular Pt electrodes. The Pt wire leads

190   for the RE and CE and a Pt wire WE (diameter: 0.5 mm) were each protected in a thin alumina

191   tube.

192

193   C. *Experimental Methods*

194   Experimental data were measured and recorded on an electrochemical workstation (model:

195   IviumStat.h, Holland). The integrated electrochemical cell loaded with 1.25 g mixed salt was

196   placed in the thermostatic zone of a SiC high-temperature tube furnace (alumina furnace tube

197   inner diameter: 40 mm). High-purity argon (99.999 pct) was introduced through the silica-gel

198   desiccant for drying at flow rates of 300 and 10 mL min^{-1} into the furnace tube from the bottom,

199   and into the YSZ tube from the top, respectively. A Pt-Rh (10 wt pct) | Pt thermocouple (Type S)

200   was employed to detect the experimental temperature. The furnace heating was programmed to

201   rise at a rate of 9 K min^{-1}. During heating, the heating program was held at 673 K and 873 K for 1

202   hour, respectively, to remove the moisture in the salt mixture, and also at 1273 K for 2 hours to

203   allow complete melting of the $CaCl_2$-NaCl-Fe_2O_3 mixture. Then, the Pt wire WE was inserted into

204   the melt, and the liquid level of the melt was determined by monitoring the open-circuit potential

205   (OCP) which became stable once the Pt wire touched the surface of the melt. The depth of the Pt

206   wire was controlled in the melt to 7 mm (contact area: 0.11 cm^2). The Ar gas in the furnace tube

207   was subsequently switched to the high-purity synthetic air (containing 20.8 pct O_2 and 79.2 pct

208   N_2) at the rate of 300 mL min^{-1}. This was to maintain a stable O_2 partial pressure outside the YSZ

209   tube that is needed for the "O^{2-} | YSZ | Pt | O_2 (air)" RE to work.
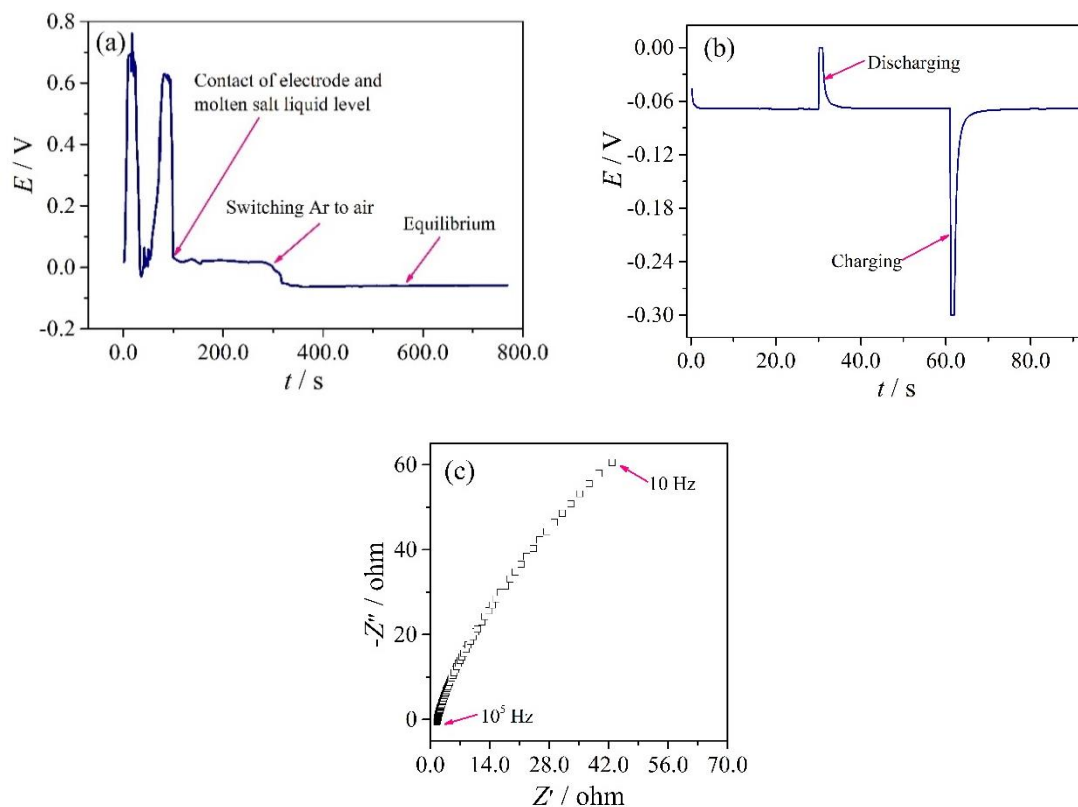
210   Figure 2(a) presents a typical OCP-time plot recorded in the course of immersing the Pt wire

211   WE into the melt and then switching from Ar to dry air in the furnace chamber. It can be observed

212   that, when the WE contacted the liquid level, the OCP instantaneously became stable. When the

213   atmosphere in the furnace tube was switched, the OCP slowly fell (the falling speed was related to

214   inner diameter of the furnace tube and the air flow rate), and finally stabilized at about -90 mV.

215   This result indicates that the "O^{2-} | YSZ | Pt | O_2 (air)" RE could work well and respond quickly to

216   the change of oxygen partial pressure in the furnace tube.

217   In order to test the reversibility of the RE in this work, a polarization experiment was also

carried out. The cell was discharged by short-circuiting, and then charged by an external current for 1 second, respectively. The WE potential responded quickly as shown in Figure 2(b). However, when the short-circuiting or the external current was removed, the WE potential returned to the initial OCP value within 3 seconds, as shown in Figure 2(b). The polarization result indicates that the "O^{2-} | YSZ | Pt | O_2 (air)" RE had a good reversibility.

After the OCP-time curve became stable, the total resistance of the melt and the YSZ membrane between the WE and RE was first measured by the alternating current (AC) impedance method (range and number of frequencies: $10^5 \sim 10$ Hz and 121, amplitude: 0.025 V, the OCP was taken as the applied bias potential). Figure 2(c) is a typical AC impedance Nyquist plot, showing a resistance of 1.64 ohm at the high frequency end, which was taken as the resistance value for the positive feedback compensation in all relevant electrochemical analyses.

Fig. 2—A typical OCP-time plot recorded in the course of immersing the Pt wire WE into the molten mixture containing 0.5 wt pct Fe_2O_3 and then switching from Ar to air in the furnace tube (*a*); a typical WE potential-time curve recorded in the polarization experiment (*b*), and a typical AC impedance Nyquist plot recorded at the OCP (bias potential) (*c*). RE: O^{2-} | YSZ | Pt | O_2 (air).

In the experiment, the OCP-time curve was always measured to determine if the cell had reached at a relatively stable state (usually, the OCP could fluctuate within 10 mV). Also, if necessary, the AC impedance measurement was repeated. It was found that the resistance from repeated measurements was fairly stable in the range of 1.64±0.08 ohm. Following these analyses,

a CV was usually recorded first, and repeated when needed, to confirm if the cell was in a stable state. Other electrochemical measurements were then conducted sequentially. No visually noticeable change for the YSZ tube used was observed after experiments. All potentials in this work were reported with reference to the " O^{2-} | YSZ | Pt | O_2 (air)" RE.

In order to examine the structural features and the morphology of the reduction products, two potentiostatic electrolysis experiments were carried out, in which a Pt wire and a Pt foil (30 mm × 2 mm × 0.1 mm) were employed as the WE, respectively. Each electrolysis experiment was carried out for 30 minutes at the reduction potential of about -0.7 V based on the CV. When using the Pt foil WE, the amount of the melt in the YSZ tube increased to 2.00 g, the area of CE on the outer surface of the YSZ increased to 4.56 cm^2, and the depth of the Pt foil in the melt was controlled to be 15 mm. Other conditions were the same as the experiments for electrochemical analyses as mentioned above.

After potentiostatic electrolysis, the Pt WE was separated from the solidified melt, and repeatedly washed, under sonication, in distilled water and absolute ethyl alcohol in succession to remove residual salts attached to the surface of the WE. A short piece was cut from the portion of the Pt wire WE immersed in the melt. It was then mounted in epoxy resin to enable examination of the cross section of the electrode by scanning electron microscopy (SEM) (Nova 400 Nano) equipped with energy dispersive spectrometry (EDS) (INCAIE 350 Penta FET X-3). For the Pt foil WE, the surface phase was analyzed by X-ray diffraction (XRD, Cu Kα, Philips Xpert Pro MPD). Due to the requirement of XRD analyses for sample size, the Pt foil was cut and re-joined to increase the width from 2 to 4 mm and decrease the length from 15 mm (original depth in the melt) to about 8 mm.

## III. RESULTS AND DISCUSSION

A. *Cyclic Voltammetry*

Figure 3(a) presents the CVs recorded in the molten CaCl$_2$-NaCl eutectic mixture with 0.5 wt pct Fe$_2$O$_3$ recorded at an increasing potential scan rate, *v*, and that recorded without Fe$_2$O$_3$ (*i.e.*, the blank melt) at 50 mV s^{-1} and 1273 K. It is observed on the CV that, within the potential range scanned, the current of the blank melt is basically zero, indicating negligible redox active impurities and good electrochemical stability of both the blank melt and the WE in this potential range. In presence of Fe$_2$O$_3$, the current on the CV smoothly increases at first with negative potential scan, and then rapidly increases to form a reduction peak C$_1$. After reversing the scan, an oxidation peak A$_1$ appears.

Because C$_1$ and A$_1$ are both absent on the CV in the blank melt, they must have been related with dissolved Fe$_2$O$_3$ and may be attributed to the reduction of the Fe^{3+} ion and the re-oxidation of the reduction product, *e.g.* Fe. The concentration of Fe$_2$O$_3$ in the molten CaCl$_2$-NaCl mixture was 0.5 wt pct which is equivalent to a mole fraction of 2.5×10^{-3}. For approximation, this mole fraction

278   was assumed to be the activity of Fe_2O_3 in the melt, while the activity of Fe on the electrode was

279   assumed to be unity. Thus, calculation of the decomposition voltage could be conducted under an

280   O_2 partial pressure of 20.8 kPa for the RE using the thermodynamic software Factsage.[48] Under

281   the applied conditions, the calculated decomposition voltage of $Fe_2O_3 \rightarrow 2Fe + 1.5O_2$ is -0.791 V

282   which is lower than that of any other component in the melt. In fact, only the oxide can be reduced

283   under the condition of the ion conducting membrane. Because all electrochemical analyses were

284   carried out against the O^{2-} | YSZ | Pt | O_2 (air) RE, it is reasonable to take the decomposition

285   voltage of -0.791 V for Fe_2O_3 as the reduction potential of Fe^{3+} to Fe. For the CVs, with some

286   basic assumptions, it can be calculated that the formal potential is -0.680 V.

287
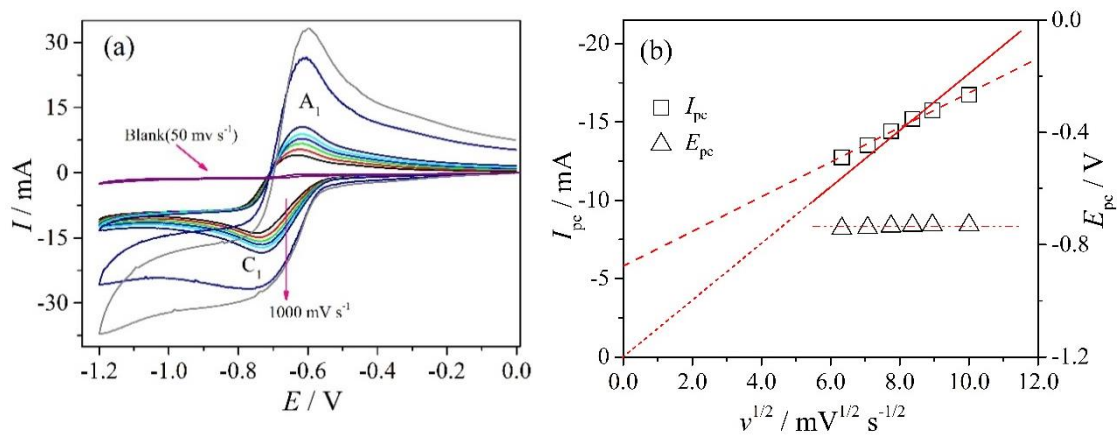
288

289   Fig. 3—CVs recorded in molten $CaCl_2$-NaCl at 1273 K with 0.5 wt pct Fe_2O_3 at v (potential scan

290   rate) = 0.04, 0.05, 0.06, 0.07, 0.08, 0.10, 0.50, or 1.00 V s^{-1}, and without Fe_2O_3 (blank) at v = 50

291   mV s^{-1} (*a*), and correlations of I_{pc} (reduction peak current) and E_{pc} (reduction peak potential) with

292    $v^{1/2}$ (*b*). RE: O^{2-} | YSZ | Pt | O_2 (air).

293

294   Since only one pair of oxidation-reduction peaks, A_1 and C_1, can be seen on the CVs in Figure

295   3(a), and the half-peak potential of peak C_1 is -0.649 V (at 40 mV s^{-1}) which is sufficiently close to

296   the calculated formal potential of -0.680 V, it is reasonable to attribute peak C_1 to the one-step

297   reduction of $Fe^{3+} + 3e \rightarrow Fe$. There may be two reasons for observed and calculated potentials for

298   peak C_1. Firstly, the actual activity of Fe_2O_3 in the melt could be larger than the mole fraction.

299   Secondly, the deposited Fe could alloy with the Pt electrode as indicated by the Fe-Pt phase

300   diagram,[49] resulting in a Fe activity lower than unity during the initial reduction.

301   As shown in Figure 3(a), electroactive species in the melt can be reduced or oxidized and the

302   corresponding redox peaks arise in the case of scanning the potential. The current of the cell, that

303   is, the oxygen-ion current passing through the YSZ membrane, does not increase/decrease at all

304   times with applied potential. Rather, it changes with the reactions of the electroactive species.

305   Obviously, the transport, including electromigration, of O^{2-} ions in the YSZ membrane does not

affect the behavior of electroactive species on the Pt WE in the three-electrode cell at a sufficiently high temperature. However, in a future industrial two-electrode cell, the transports of oxygen ions through the YSZ membrane may be highly likely an important factor affecting the rate of the overall process. It is worth noting that the shapes of peaks C_1 and A_1 on the CVs indicate that the reduction products could be soluble,[50] and the physical state of the reduction products will be analyzed later by means of correlation detection.

In order to evaluate the reversibility of electrode process, the CV tests were performed at different scan rates. Figure 3(a) shows that with the potential scan rate increasing from 0.04 to 0.1 V s^{-1}. The ratio of the oxidation and reduction peak currents (base current subtracted), I_{pa}/I_{pc}, is close to unity, the reduction peak potential, E_{pc}, remains constant ($\sim$ -0.735 V) with increasing v, while plotting I_{pc} vs $v^{1/2}$ produces a straight line whether or not the origin is passed, as shown in Figure 3(b). These three observations indicate that the reduction of Fe^{3+} to Fe is diffusion controlled and reversible.[6,50,51] However, when v increases from 0.1 to 0.5 $\sim$ 1.0 V s^{-1}, E_{pc} shifts negatively, and I_{pc} deviates noticeably from the $I_{pc} - v^{1/2}$ fitting straight line (the data from high scan rates are not included in Figure 3(b), and I_{pa}/I_{pc} increases beyond 1. These CVs which result from the reduction reaction of Fe^{3+} to Fe on the Pt electrode show the reversible shape at low scan rates but the CV shape become less reversible or irreversible with increasing the scan rate.[52] A supplementary discussion on the reversibility of the reduction process is added in Section III−E.

To sum up, the reduction of Fe^{3+} to Fe on the Pt WE as represented by the CVs recorded at relatively low potential scan rates is a one-step and diffusion-controlled reversible process. This finding is consistent with the reported CVs of Fe^{3+} in molten $CaCl_2$-NaCl with molybdenum and silver wires as the WE and RE, respectively, although the I_{pa}/I_{pc} ratio on the reported CVs was not unity.[6] It is acknowledged that it is yet uncertain whether the reduction-produced Fe was dissolved in the melt or alloyed with the Pt WE. It is also necessary to check if there was any reduction product and its physical state on the Pt WE before the CVs could be evaluated properly. Hence, three measures were taken as described below.

Firstly, reversal CP was applied to investigate the redox couple of Fe^{3+}/Fe in the melt and the findings are shown in Figure 4(a). It can be seen that upon application of the constant negative current, the potential fell initially and soon arrived at a plateau. The plateau potential, ca. -0.8 V, is consistent with the potential of the Fe^{3+} reduction peak shown in Figure 3(a).

The shape of the reversal CP can be explained as follows. With the Fe^{3+} concentration decreasing in the melt, the diffusion of Fe^{3+} to the electrode surface becomes slower than the depletion of Fe^{3+} on the electrode surface. When the Fe^{3+} concentration on the electrode surface falls to zero, the electrode potential changes quickly to more negative value where the next reduction reaction occurs. Then, when an equal reverse current I is applied, the potential also reverses quickly till another plateau where the previous reduction products are re-oxidized to Fe^{3+}. The difference between the applied currents is very small, and the amount of reduction products is also very small. Also, the reduction-produced Fe dissolves into the Pt electrode to form a solid

solution (for details, see the follow – up). Thus, there is little difference in the activity of Fe on the surface of the solid solution, leading to very comparable overpotentials of the re-oxidation, as shown in Figure 4(a). The tilt of the re-oxidation plateau indicates that the activity of iron in the alloy decreases continuously during oxidation, which could be due to the fact that the Fe diffused into the Pt electrode was not oxidizable on the time scale of the CV. Upon completion of the re-oxidation of the reduction produced Fe on the electrode surface, the potential quickly changes to more positive values of about +0.2 V. It is supposed to be the oxidation of oxygen ions to oxygen molecule at potentials of about +0.2 V, where some fluctuations can be observed in Figure 4(a), indicating the gas involved in the electrode reaction. This is related to the oxidation of the oxygen ion: $O^{2-} \rightarrow 1/2O_2 + 2e$. It should be noted that oxidation of oxygen ions in the melt was not further investigated in the positive potential range because the present work dealt mainly with the reduction of iron ions in the negative potential range.
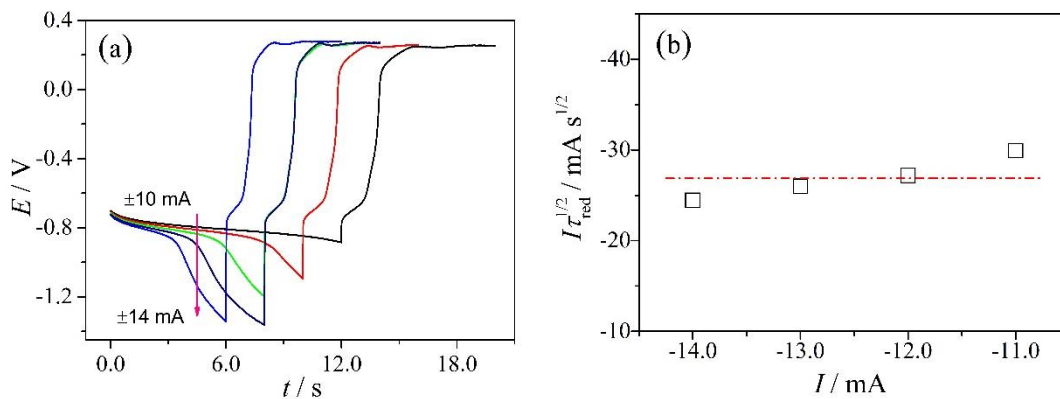

Fig. 4—Reversal CPs on the Pt WE in molten $CaCl_2$-NaCl with 0.5 wt pct Fe_2O_3 at 1273 K and different currents (±10, ±11, ±12, ±13 and ±14 mA) (*a*) and the correlation of the $I\tau^{1/2}$ (τ: transition time) value against the cathodic current *I* for the reduction plateau (*b*). RE: O^{2-}| YSZ | Pt | O_2 (air).

The transition time for reduction or oxidation (τ_{red} or τ_{ox}) is basically the duration of the potential plateau in Figure 4(a). The data listed in Table I were measured using methods in accordance with the literature.[53-55] It can be seen from Table I that, at 1273 K, increasing the applied current led to a quicker depletion of electroactive ions on the electrode surface, resulting in decreased values of τ_{red} and τ_{ox}. Table I also shows that the τ_{red}/τ_{ox} ratio also decreased from 6 to 2.9, suggesting that increasing the applied current has a greater impact on the decrease of τ_{red} than that of τ_{ox}. According to the literature,[55] at $\tau_{red}/\tau_{ox} = 1$, the reduction products should be insoluble; when $\tau_{red}/\tau_{ox} = 3$, soluble reduction products, usually in the liquid electrolyte, would be expected. In this work, however, $\tau_{red}/\tau_{ox} = 6 \sim 2.9$ ($\tau_{red}/\tau_{ox} = 7$ was reported in the literature [55]) which makes it uncertain if the reduction products were insoluble (*e.g.* Fe) or soluble (*e.g.* Fe^{2+}).

374   Secondly, some experiments were carried out. In these experiments, upon confirmation of the

375   electrochemical cell having reached the equilibrium or steady state as indicated by the OCP,

376   potentiostatic electrolysis was performed at -0.76 V for a predetermined time of 30 seconds. Then,

377   the OCP was monitored for 60 seconds (halting time), while the Pt WE was in two working modes:

378   the usual static mode and the manually rotating mode with 2 circles. Then, anodic LSV was

379   performed from -0.9 to 0 V at v = 50 mV s^{-1}. The same procedure was repeated for another two

380   predetermined times (60 and 90 seconds) of electrolysis at -0.76 V. Thus, the experiments

381   produced six LSVs, as shown in Figure 5. In inset of Figure 5, typical curves of the potentiostatic

382   electrolysis using the Pt wire WE for 30, 60, and 90 seconds are presented. In order to eliminate

383   the influence of the residual products from the reduction, before the next test, the potentiostatic

384   electrolysis was performed at 0.05 V for 90 seconds to oxidize all the materials deposited on the

385   electrode surface in the previous test, where preliminary experiments indicated that the electrode

386   was not oxidized and no new oxidation peak occurred. In addition, the preliminary experiments

387   also indicated that the halting time from 15 to 360 seconds had no detectable effect on the LSVs

388   recorded in the static mode.

389
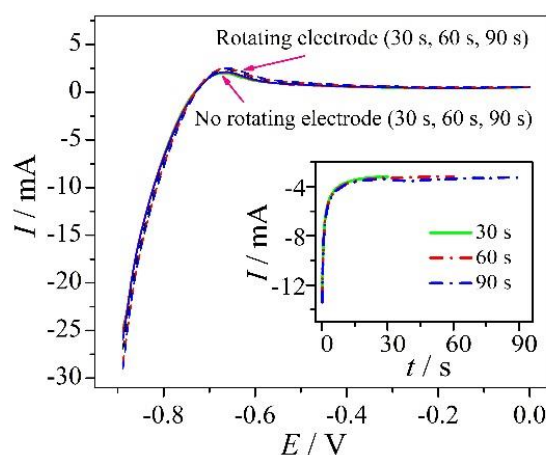
390

391   Fig. 5—LSVs recorded at 50 mV s^{-1} on the Pt wire WE under the static and rotating modes after

392   the potentiostatic electrolysis for 30, 60, 90 seconds in molten CaCl$_2$-NaCl with 0.5 wt pct Fe$_2$O$_3$.

393   Inset: a set of typical current-time curves of potentiostatic electrolysis using the Pt wire WE for 30,

394   60, 90 seconds. Potentiostatic electrolysis potential: -0.76 V; time: 30, 60, 90 s; temperature: 1273

395   K; RE: O^{2-}| YSZ | Pt | O$_2$ (air).

396

397   It is expected from these experiments that if the reduction products were soluble, they would

398   not accumulate on the electrode surface and, consequently, no significant change on the anodic

399   LSV would happen in the static mode even if the time of the potentiostatic reduction was doubled.

400   Otherwise, if insoluble products were formed, doubling the time of the potentiostatic reduction

401   should lead to likely a double increase of the re-oxidation current. If the Pt WE was rotated

402   manually when measuring the OCP for 60 seconds (halting time), for reduction products soluble in

the melt, the diffusion flux of the products from the electrode surface into the melt would decrease in the following anodic LSV. However, if the reduction product could remain on the Pt WE due to alloying with Pt, the diffusion flux of the products from the surface into interior of the Pt WE would not markedly change. The current on the following LSV should correspond to the change of the diffusion flux. Consequently, following the potentiostatic reduction and the 60-second OCP measurement with the rotating Pt WE, changes of the oxidation peak on the anodic LSV can be used to judge if the reduction products dissolved in the melt.

As can be observed in Figure 5, the anodic LSVs are highly consistent with each other under various conditions. Under the static mode, doubling the time of potentiostatic electrolysis did not lead to a higher current of the oxidation peak on the LSVs, suggesting that the reduction products could be soluble. However, it cannot be determined whether the reduction products dissolved in the melt or alloyed with the Pt electrode. Further, Figure 5 shows that the oxidation peak currents on the LSVs are also the same with or without rotating the Pt WE, indicating the reduction products having alloyed with Pt.

Thirdly, the Pt WE was characterized by SEM, EDS, and XRD after the potentiostatic electrolysis to identify the reduction products. Figure 6 shows the SEM image of the cross section of the Pt wire WE, the corresponding EDS, and the line scanning analyses of Pt, Fe, and O. As shown in Figure 6(b), the EDS analysis confirmed the presence of Fe on the Pt wire WE surface. Figure 6(d) presents the line scanning profile for Fe, confirming a maximum Fe content at the position of 0.5 μm from the Pt WE surface. Figure 7 shows the XRD pattern for the Pt foil WE after potentiostatic electrolysis. From Figure 7, the existence of the $FePt_3$ phase is not certain, but the independent pure Fe phase can be excluded. Therefore, based on the EDS analyses, it is believed that reduction-produced Fe could have reacted with the Pt electrode to form an alloy or intermetallic compound, $e.g.$, $FePt_3$ whose XRD pattern overlaps with that of Pt.
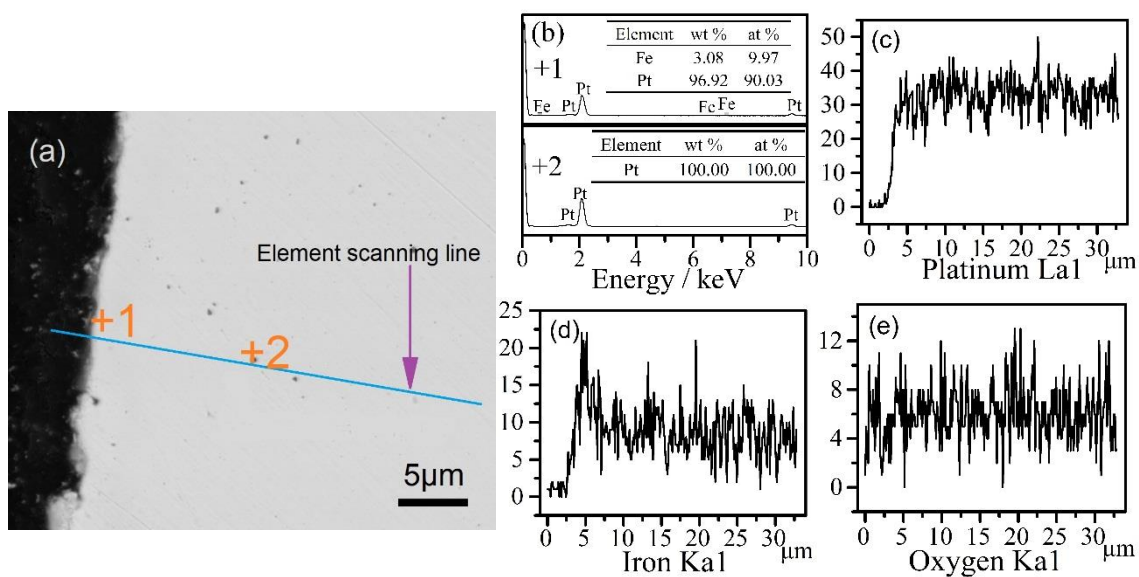
432 Fig. 6—SEM image of the cross section of the Pt wire WE (*a*), EDS analyses of spots 1 and 2 in

433 the SEM image (*b*), and the line scanning profiles of Pt (*c*), Fe (*d*), and O (*e*) after potentiostatic

434 electrolysis in molten $CaCl_2$-NaCl with 0.5 wt pct Fe_2O_3. Potentiostatic electrolysis potential: -

435 0.73 V; time: 30 min; temperature: 1273 K; RE: O^{2-} | YSZ | Pt | O_2 (air).

436

437 The findings from SEM, EDS, and XRD are in agreement with that from the reversal CPs and

438 the LSVs, confirming the reduction products to be Fe which, upon deposition, alloyed with the Pt

439 WE. However, the fact that $I_{pa}/I_{pc} \approx 1$ as shown in Figure 3(a) suggests that the alloy formation

440 had not caused a major impact on the derived parameters from the CVs.

441
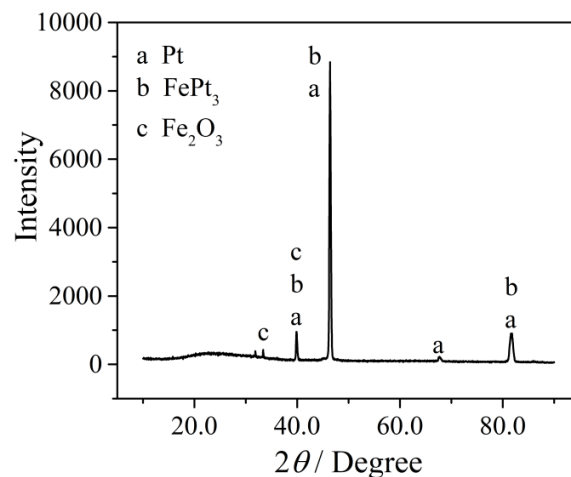
442

443 Fig. 7—XRD pattern for the Pt foil WE after potentiostatic electrolysis in molten $CaCl_2$-NaCl

444 with 0.5 wt pct Fe_2O_3. Potentiostatic electrolysis potential: - 0.7 V; time: 30 min; temperature:

445 1273 K; RE: O^{2-} | YSZ | Pt | O_2 (air).

446

447 For a reversible electrode process with both soluble reactant and product, considering only

448 semi-infinite linear diffusion, the number of exchanged electrons in the electrode reaction and the

449 diffusion coefficient are usually calculated, respectively, from Eq. [1] and the Randles-Sevcik

450 equation, that is, Eq. [2].[56-60]

451 $|E_p - E_{p/2}| = 2.2RT/(nF)$ [1]

452 $I_{pc} = - 0.4463nFAC_0(RT)^{-1/2}(nFvD)^{1/2}$ [2]

453 where E_p is the cathodic or anodic peak potential, V; $E_{p/2}$ the half-peak potential, V; n the number

454 of exchanged electrons; F Faraday's constant, F = 96500 C mol^{-1}; R the molar gas constant, R =

455 8.314 J mol^{-1} K^{-1}; T the temperature, T = 1273 K; A the area of WE, here A = 0.11 cm^2; D the

456 diffusion coefficient of electroactive species (Fe^{3+}), cm^2 s^{-1}; I_{pc} the cathodic peak current, A; v the

457 potential scan rate, V s^{-1}; and C_0 is the molar concentration of electroactive species (Fe^{3+}), mol

458 cm^{-3}. In this work, due to the very low Fe_2O_3 concentration (C_0 = 1.10×10^{-4} mol cm^{-3}), the density

459 of the molten $CaCl_2$-NaCl mixture with Fe_2O_3 at 1273 K can be expressed approximately by that

of the molten mixture alone (1.758 g cm^{-3}).[61] It is assumed that the corrections related to cylindrical geometry of the Pt wire WE can be neglected under the experimental conditions.

Specifically, in this work, the CVs showed three typical characteristics for reversible electrode reactions justifying the use of Eqs. [1] and [2]. The EDS and XRD analyses show that the reduction product does not exist in the form of an independent Fe phase, but rather forms an alloy with the electrode. Here, the alloy formed between the precipitated Fe and the Pt electrode can be regard as a solid solution. In other words, the reduction product is dissolved in the Pt electrode, not an insoluble deposit. More importantly, the alloy formation was found to have no significant effect on the above typical characteristics of reversible reaction. Therefore, Eqs. [1] and [2] were applied to the reversible reaction with soluble reactant although the reduction product Fe was not dissolved in the electrolyte but in the Pt electrode.

The numbers of exchanged electrons in the reaction of the cathodic and anodic peaks as derived from Eq. [1] are $n_c = 2.6 \approx 3$ and $n_a = 2.8 \approx 3$, respectively. It can then ascertain that, on the CVs, the cathodic peak corresponds to the one-step reduction of Fe^{3+} to Fe, and the anodic peak to the re-oxidation of Fe to Fe^{3+}.

For a diffusion-controlled reversible reaction, it is well known that the relationship between I_{pc} and $v^{1/2}$ accords with the Randles-Sevcik equation, that is, Eq. [2]. According to Eq. [2], theoretically, the linear relationship between I_{pc} and $v^{1/2}$ should pass through the origin. However, quite a few researchers found that was not the case, if only experimental data points were fitted in a straight line. The discussion is as follows:

Firstly, there is some accompanying process (such as ion adsorption) in the electrode reaction, which is parallel to the main Faraday process.[2,62,63] In this case, the experimental data points, excluding the origin, are fitted in a straight line and the intercept with a small positive value can be obtained. These small positive values for intercepts cannot invalidate the deduction regarding that the process is diffusion controlled. This fitting method is adopted by some researchers. [2,62,63]

Secondly, there is a certain experimental error.[64] In this case, according to Eq. [2], theoretically, the linear relationship between I_{pc} and $v^{1/2}$ should pass through the origin. Therefore, in order to reduce the error, the experimental data points, together with the origin point, are fitted in a straight line within a desired accuracy. This fitting method is also adopted by some researchers.[53,54,64,65] It should be noted that the approach is theoretically in line with the requirements of the Randles-Sevcik equation.

In this work, since both the parallel process of electrode reaction and experimental error are considered to be uncertain, the experimental data points are fitted into a straight line with and without passing through the origin for the convenience of comparison, as shown in Figure 3(b). Thus based on Eq. [2], the diffusion coefficients can be derived from the slopes of linear fitting of the $I_{pc} - v^{1/2}$ plot. They are found to be $(4.9\pm0.5)\times10^{-5}$ cm^2 s^{-1} (passing through the origin) and $(1.8\pm0.1)\times10^{-5}$ cm^2 s^{-1} (not passing through the origin), respectively. The difference between the two is not large and the two diffusion coefficient values are in the same order of magnitude.

499   B. *Square Wave Voltammetry*

500   Due to its high sensitivity, SWV is effective in suppressing the influence of the capacitive

501   background current as often observed on CV, particularly at relatively high scan rates. In this

502   experiment, in order to confirm the reversibility of electrode process and evaluate electrochemical

503   parameters such as the number of transferred electrons and diffusion coefficient, the SWV tests

504   were performed at different scan frequencies. The SWVs of the melt containing 0.5 wt pct Fe_2O_3

505   (including the blank melt) at 1273 K were measured at 1 mV in step potential and 30 mV in

506   amplitude, and different scan frequencies, as shown in Figure 8(a).
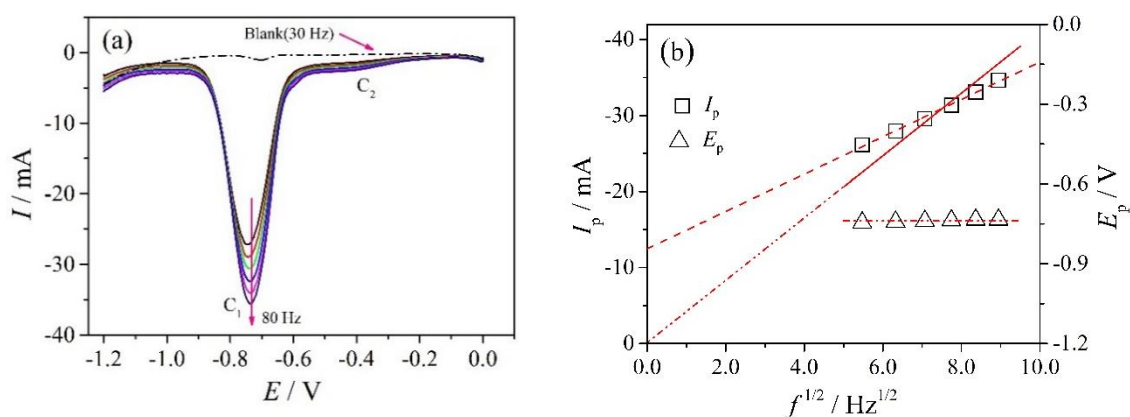
507
508
509   Fig. 8—SWVs recorded in the molten $CaCl_2$-NaCl mixture with 0.5 wt pct Fe_2O_3 at different

510   frequencies (30, 40, 50, 60, 70, 80 Hz) and 1273 K (*a*) and the correlations between the peak

511   current (I_p), the peak potential (E_p), and the square root of the frequency ($f^{1/2}$) , respectively (*b*).

512   RE: O^{2-} | YSZ | Pt | O_2 (air).

513

514   Figure 8(a) shows that with negative scanning of the potential, the current starts to smoothly

515   increase, experiences a small peak C_2 first at -0.4 V, and then rapidly increases to the main

516   reduction peak C_1 at -0.74 V. The potential of C_1 is consistent with that of the reduction peak C_1

517   on the CVs in Figure 3(a), indicating its origin being the Fe^{3+} reduction. The peak C_2 in Figure 8(a)

518   is invisible on the blank SWV, and neither on the CVs in Figure 3(a), and hence the formation of

519   peak C_2 should have a relation with addition of Fe_2O_3. Frangini *et al.* [66] found that the addition of

520   0.5 mol pct La_2O_3 to the molten carbonate salt resulted in a dramatic increase of O_2 solubility.

521   Similarly, it is supposed that the addition of Fe_2O_3 could increase O_2 solubility in the melt in this

522   work. It is known that the dissolution of oxygen could lead to the formation of superoxide and

523   peroxide ions in molten salts at high temperatures and these ions could keep a dynamic

524   equilibrium of formation and dissociation.[66-69] Therefore, the peak C_2 might be ascribed to the

525   related reduction reaction of oxygen in the melt. Here the related reduction reaction of oxygen

526   means the reduction of intermediate oxide ion species such as superoxide and peroxide ions rather

527   than to simply molecular oxygen entities. However, the occurrence of the peak C_2 still needs to be

528   further explored.

529   With increasing the frequency f, the potential of Fe^{3+} reduction peak C_1 basically remains

530   unchanged; by plotting and fitting the relation between the reduction peak C_1 current I_p (base

531   current subtracted) and the square root of the frequency $f^{1/2}$ value, a linear correlation between I_p

532   and $f^{1/2}$ is observed whether or not the origin is passed, as shown in Figure 8(b). It can

533   comprehensively be judged that the reduction of Fe^{3+} corresponding to the peak C_1 is a reversible

534   reaction in the melt with 0.5 wt pct Fe_2O_3 at 1273 K. Thus, within the range of the frequencies

535   measured, the number of exchanged electrons and the diffusion coefficient of Fe^{3+} ions can be

536   calculated from Eqs. [3] [53,54,58, 60,70,71] and [4], [72-76] respectively, as follows:

537    $W_{1/2} = 3.52RT/(nF)$ [3]

538    $I_p = - 0.31\pi^{-1/2}R^{-1}T^{-1}AC_0D^{1/2}n^2F^2\Delta Ef^{1/2}$ [4]

539   where $W_{1/2}$ is the half-peak width, V, the peak is not exactly symmetric as predicted by theory, see

540   the method from the literature [71] for taking $W_{1/2}$ value; f the frequency, Hz; and ΔE is the

541   potential amplitude, V, here $\Delta E = 0.03$ V. Eqs. [3] and [4] are applicable to the reversible system

542   with semi-infinite linear diffusion. It is known that Eq. [3] is valid if the peak current is linear with

543   the square root of the frequency of the potential signal in SWV.[53,54,71] And Eq. [4] can be applied

544   when the potential amplitude (ΔE) (30 mV in this work) in the SWV is smaller than the ratio of

545    $RT/(nF)$.[74-77]

546   Based on Eq. [3], it can be derived from the fitting that the number of exchanged electrons n

547    $= 2.7 \approx 3$, which suggests again this reduction peak C_1 corresponding to the reaction of one-step

548   reduction of Fe^{3+} to Fe. In this work, similar to the above plot of I_{pc} against $v^{1/2}$ in the CVs (see

549   Figure 3(b)), it can also be understood that a plot of I_p against $f^{1/2}$ yields a straight line with and

550   without passing through the origin within a desired accuracy based on Eq. [4], as shown in Figure

551   8(b). The diffusion coefficients derived from $I_p - f^{1/2}$ fitting straight line slope are $(6.7\pm0.4)\times10^{-5}$

552    $cm^2 s^{-1}$ (passing through the origin) and $(2.4\pm0.1)\times10^{-5}$ $cm^2 s^{-1}$ (not passing through the origin),

553   respectively. The two are also close and in the same order of magnitude.

554

555   C. *Chronopotentiometry*

556   In order to determine whether the electrode process is controlled by diffusion, the CP tests

557   were performed at different applied currents. Figure 9(a) shows the CPs recorded in the melt with

558   0.5 wt pct Fe_2O_3 at 1273 K. It can be found that the characteristics on the CPs are exactly the same

559   as that of reduction part on the reversal CPs (see Figure 4(a)) mentioned above. With increasing

560   negative applied current, the depletion rate of Fe^{3+} on the surface of the electrode was quickened,

561   and the reduction transition time τ also decreased slowly. Select easily readable data on reduction

562   transition time, and draw the $I - I\tau^{1/2}$ plot, as shown in Figure 9(b).

563   From Figure 9(b), it can be observed that the measured $I\tau^{1/2}$ value varied insignificantly with

564   the applied current I and matched closely to a horizontal straight line within a desired accuracy.

565   Therefore, it can also be determined that the reduction of Fe^{3+} to Fe is a diffusion-controlled

17

process in the melt with 0.5 wt pct Fe_2O_3 at 1273 K. Based on the Sand Equation (Eq. [5]),[53-55,59,60] the diffusion coefficient of Fe^{3+} is derived to be $(7.5\pm0.6)\times10^{-5}$ cm^2 s^{-1}.

$$I\tau^{1/2} = - nFAC_0\pi^{1/2}D^{1/2}/2 \qquad\qquad [5]$$

where I is the cathodic current (A); τ is the transition time (s). Eq. [5] is applicable to the case where the mass transport is controlled by semi-infinite linear diffusion at constant applied currents. It should be noted that the application of Eq. [5] is not dependent on the reversibility of reaction.
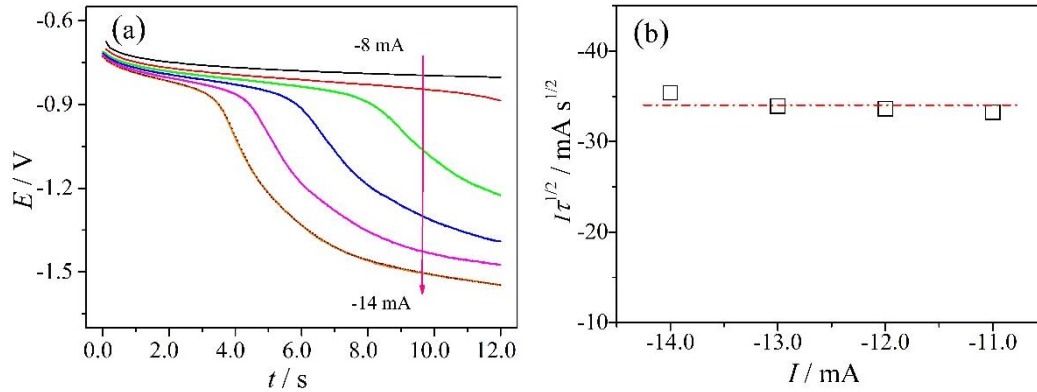
Fig. 9—CPs recorded in the melt with 0.5 wt pct Fe_2O_3 at 1273 K at different cathodic currents of -8, -10, -11, -12, -13, -14, -14 mA (*a*) and the correlation between the cathodic current I and the $I\tau^{1/2}$ (τ: transition time) value for the reduction plateau (*b*). RE: O^{2-} |YSZ | Pt | O_2 (air).

In addition, it can be observed from Figure 9(a) that there is another reduction reaction at about -1.25 to -1.55 V. The attribution of the reduction reaction can be analyzed as follows:

In this work, since the YSZ membrane is used as the isolation membrane, only the iron ions from the added iron oxide can be electrolytically reduced in the melt; the chloride cannot be reduced. Besides Fe_2O_3 in the melt, there may also be a small amount of oxide impurities or newly formed oxides, such as FeO, Na_2O, and CaO. FeO is derived from the decomposition of Fe_2O_3; Na_2O and CaO are derived from the chlorination reaction of NaCl-$CaCl_2$ with Fe_2O_3. Their production should be small. However, the theoretical decomposition potentials of CaO and Na_2O calculated from the thermodynamic software Factsage [48] are about -2.9 V and -2.6 V, respectively, which are far more negative than -1.55 V. The theoretical decomposition potential of FeO is -1.32 V, so the reduction at about -1.25 to -1.55 V is considered to be the reduction of Fe^{2+} to Fe. Unfortunately, the reduction reaction at about -1.25 to -1.55 V was not investigated in this work.

Further analysis of the reversal CPs (see Figure 4(a)) is to determine the reduction transition time and plot the I –$I\tau^{1/2}$ relation. The plot compares closely to a horizontal linear relation, as shown in Figure 4(b). Likewise, based on the Sand Equation (Eq. [5]), the diffusion coefficient of Fe^{3+} ions is derived to be $(7.5\pm0.7)\times10^{-5}$ cm^2 s^{-1}, which is utterly consistent with that from Figure 9(b). It is noteworthy that the CP at -14 mA is tested twice, and complete superposition of two

corresponding curves is observed, as shown in Figure 9(a). Almost exactly the same values of the diffusion coefficient obtained from the CPs (Figure 9(b)) and the reversal CPs (Figure 4(b)) as well as the results of repeated test of the CP at -14 mA shown in Figure 9(a) suggest that the experimental cell system is stable in nature, with excellent reproducibility and reliable result of electrochemical test.

D. *Chronoamperometry*

In order to observe nucleation behavior and confirm whether the electrode process is controlled by diffusion, the CA tests were performed at different applied potentials. Figure 10(a) displays the CAs recorded in the melt with 0.5 wt pct Fe_2O_3 at 1273 K, from which no nucleating behavior is observed,[7,9,78] possible due to alloying of reduction product Fe and the electrode. It can be inferred that no nucleation controlled the kinetics of the electrodeposition mechanism of iron in the eutectic $CaCl_2$-NaCl melt at 1273 K. When the step potential is applied on the WE, three cases can be observed with corresponding limited current I_{lim}. Firstly, when the step potential is low (-0.5, -0.6 V), the limited current I_{lim} is approximately equal to zero, and this is because the step potential is not high enough to trigger the reduction reaction of Fe^{3+}, together with electronic conduction current and current produced by reduction of foreign ions. Secondly, when the step potential reaches -0.7 V, the current quickly falls in initial period, indicating deposition reaction of Fe^{3+}; this step potential is utterly consistent with the reduction potential of Fe^{3+} observed by CV, SWV, and CP described above, with notable increase of the limited current, but not reaching the maximum stable value. Thirdly, with negative increase in the step potential, the current quickly falls in the initial period. This is because of the deposition reaction of Fe^{3+} on the Pt WE leading to rapid decrease of Fe^{3+} concentration near the electrode, to the extent it is too late for Fe^{3+} in the melt to diffuse to the surface of WE, resulting in sharp attenuation of current; then, the current slowly decreases and remains stable at I_{lim}. At this time, the diffusion of Fe^{3+} ions to the surface of the WE reaches the balance with the deposition.
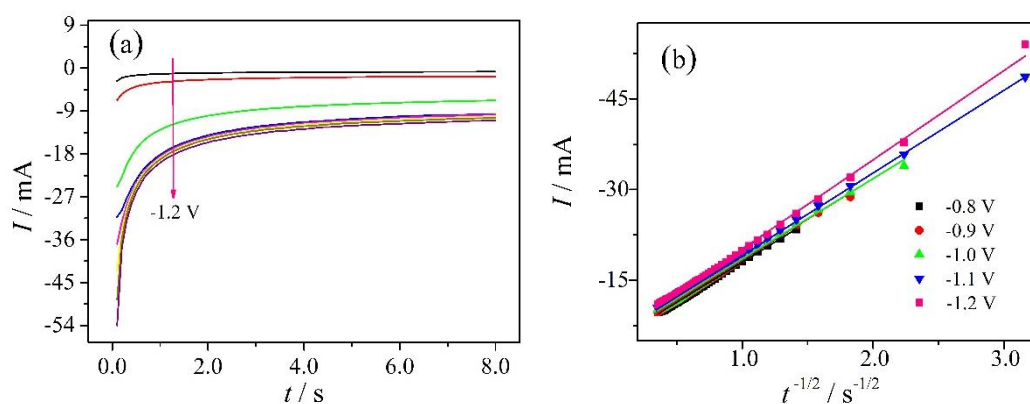
Fig. 10—CAs recorded in the melt with 0.5 wt pct Fe_2O_3 at 1273 K at different step potentials of -0.5, -0.6, -0.7, -0.8, -0.9, -1.0, -1.1, -1.2 V (*a*) and the correlation between the cathodic current *I* and the $t^{-1/2}$ value at different step potentials of -0.8, -0.9, -1.0, -1.1, -1.2 V (*b*). RE: O^{2-} |YSZ | Pt |

19

626   O_2 (air).

627

628   It can be inferred that the reduction reaction at the applied potentials from -1.0 to -1.2 V in

629   Figure 10(a) is not the same as that at the second plateau potentials from -1.25 to -1.55 V in Figure

630   9(a). The explanation is as follows:

631   Firstly, from Figure 10(a), the negative shift in potential from -0.8 to -1.2 V does not affect

632   the value of the current. Thus, the stable currents at these potentials (where the diffusion reached

633   the limit rate) have little difference, but are larger than that at -0.7 V (where the diffusion did not

634   reach the limit rate). The reduction reaction taking place at potentials from -0.7 to -1.2 V should be

635   the same. Under the experimental conditions, it is obviously unreasonable that the reaction at -0.7

636   V was considered as the reduction of Fe^{3+} to Fe and that at the adjacent potentials from -0.8 to -1.2

637   V as another reduction reaction.

638   Secondly, in Figure 9(a), when the applied current is in the range of -11 to -14 mA, the

639   second potential plateau on the CPs appears in the range from -1.25 to -1.55 V in addition to the

640   first potential plateau at about -0.8 V. It can be seen that the potential plateau resulted from an

641   applied current is not the only one in the CPs. That is, the reactions at different potential plateaus

642   cannot be determined directly by only the applied current in the CPs. Similarly, the reactions

643   cannot be determined directly by only the stable currents in the CAs and should be judged in

644   conjunction with the applied potential. It is noted that the second plateau potential in the CPs is

645   more negative than the applied potentials from -0.8 to -1.2 V in the CAs. Therefore, the reaction at

646   applied potentials from -0.8 to -1.2 V in the CAs should be different from that at the plateau

647   potentials from -1.25 to -1.55 V corresponding to the applied currents from -11 to -14 mA in the

648   CPs. Moreover, in this work, there is no *IR* compensation in the CAs, so that the corresponding

649   reaction at the applied potentials from -0.8 to -1.2 V actually takes place at a less negative

650   potential, which approaches the reaction potential revealed by the CVs, the SWVs, and the CPs,

651   and widens the gap from the second plateau potential.

652   For the part of data involving Fe^{3+} reduction and the limited current reaching maximum

653   stable value (*i.e.*, above-mentioned case 3) in Figure 10(a), draw corresponding $I - t^{1/2}$ curve, as

654   shown in Figure 10(b). It is seen that within the range of 0.5～8 seconds, $I - t^{1/2}$ is in good linear

655   relation, suggesting the reduction of Fe^{3+} to Fe is a diffusion controlled process within the range.

656   The diffusion controlled current conforms to the Cottrell Equation (Eq. [6]): [1,79]

657    $I = - nFAC_0 D^{1/2} \pi^{-1/2} t^{-1/2}$ [6]

658   where t is the electrolysis time, seconds. Eq. [6] is analogous to Eq. [5]. It is applicable to the case

659   where the mass transport is controlled by semi-infinite linear diffusion at a constant applied

660   potential.

661   Based on Eq. [6] and fitting $I - t^{1/2}$ straight line part in Figure 10(b), the diffusion coefficients

662   at variable step potentials are calculated from the slopes of fitting the straight line. Final diffusion

663   coefficient value is obtained as $(4.8\pm0.2)\times10^{-5}$ cm^2 s^{-1} by horizontal fitting the diffusion

664   coefficients of Fe^{3+} at each step potential.

665

666   E. *Supplementary Discussion*

667   Table II collects the diffusion coefficients of Fe^{3+} derived from multiple testing techniques

668   such as the CV, the SWV, the CP, and the CA in this work. These values are found to be

669   consistent in allowable error, despite of different measuring principles and methods, suggesting it

670   is rational to have the experimental data processed with related equations described above.

671   Although these equations come from the classical electrochemistry where they are mostly

672   established in aqueous solutions, it is known that molten salts like aqueous solutions are also

673   electrolyte solutions, so that the equations can be used to analyze electrochemical data obtained in

674   molten salts when the application conditions on these equations are satisfied. Also, the diffusion

675   coefficients of Fe^{3+} reported in related literature are compared in Table II. Taking into account

676   different experimental conditions and test methods, it is believed that the results described herein

677   match well with recorded values of the literature, suggesting our research methods are feasible to

678   build the integrated electrochemical cell with zirconia-based solid electrolyte tube.

679   It should be noted that the reversibility of an electrode reaction depends on if the ratio of the

680   product and reactant activities obeys the Nernst equation at the electrode/electrolyte interface, but

681   not by the form of the reaction product. When the reaction product is in a solid phase, its activity

682   at the electrode/electrolyte interface would be either constant (pure metal or intermetallic

683   compound) or variable (alloy). Thus, the reversibility can still be checked by the CV and the

684   SWV.[80] In this work, the obtained CVs have three typical characteristics of a reversible reaction,

685   although reduction product Fe forms an alloy with the Pt electrode. These CV features indicate

686   that alloying has no significant effect on the reversibility of reduction reaction. The calculated

687   results from the CV, the SWV, the CP, the reversal CPs, and the CA, including the number of

688   exchanged electrons and the diffusion coefficient of ferric ions, are in agreement with each other,

689   indicating that the conclusion on the reversibility of the electrode process is reasonable under the

690   present conditions.

691   In this work, Pt was chosen as the WE mainly due to its better chemical and electrochemical

692   stability against oxidation in molten salt although it formed the alloy with reduction product Fe. It

693   should be pointed out that the experimental results with good stability and reproducibility are

694   obtained when the Pt electrode is used as the WE. The authors also acknowledge that it still

695   remains a great challenge to find the suitable inert electrode for electrolytic reduction of iron oxide

696   to iron in molten electrolytes. It is known that graphite reacts with Fe$_2$O$_3$ in the melt at the

697   working temperature and hence cannot be used as the WE in this work. On the other hand, the

698   effort to use other WE materials, including low carbon steel, molybdenum, and tungsten, is still

699   ongoing and we hope to publish the findings separately in the near future.

700   In addition, the key part of the integrated cell is the YSZ tube. It is understandable that the

stability of the YSZ in the molten salt is a basic necessity to obtain reliable experimental results. In this work, the experimental time in one measurement during one thermal cycle usually lasted for about six hours at high temperatures. In the experiment, erosion of the YSZ tube was never visible, and the reproducibility and consistency of the experimental results not only showed that there was no erosion, but also showed that the RE was stable. Unfortunately, long time electrolysis tests were not performed in this work. It should also be possible to maintain the stability of the RE within a desired accuracy for a long time in practice.

It should also be noted that the working temperature of 1273 K studied in this work seems a little too high when heat loss and salt evaporation are significant. However, higher temperatures will also bring about both thermodynamic (lower Gibbs free energy) and kinetic (faster reaction) benefits to the electrode reactions, in addition to the higher conductivity of the YSZ membrane. It is common knowledge that for the same number of joules, electric energy and reaction energy are both of higher prices than that of heat. Thus, from the viewpoint of energy economy, a higher working temperature is not necessarily more expensive for an electrolytic process. The salt loss *via* vaporization at higher temperatures could, however, be problematic, but the liquid mixture of $CaCl_2$ and NaCl is expected to deviate from the ideal mixture, and hence evaporate less than the pure component salt alone at the same temperature. We also anticipate a lower vapor pressure of the mixture of molten salts when the concentration of dissolved metal oxides approaches to saturation. In addition, the operating temperature is considered not to be the focus in the work because it is limited by some factors such as the resistance of YSZ tube. For the case in this work, if the wall of YSZ tube used became thinner, or Y_2O_3 and Yb_2O_3 co-doped zirconia tube was employed, [81,82] so as to decrease the resistance of zirconia membrane, the operating temperature of the integrated cell would be lower than 1273 K, and the evaporation of molten salt would also reduce.

IV. CONCLUSIONS

A unique integrated three-electrode cell with the "O^{2-} |YSZ | Pt | O_2 (air)" RE was constructed using yttria-stabilized zirconia (YSZ) solid electrolyte tube with a closed end. Electrochemical behavior of ferric ions was systematically investigated in the molten $CaCl_2$-NaCl eutectic mixture containing 0.5 wt pct Fe_2O_3 at 1273 K. The test results of various electrochemical techniques, such as CV, LSV, SWV, CP, reversal CP, CA, suggest that the reduction of Fe^{3+} to Fe on the Pt WE could be a single one-step and diffusion-controlled reaction that was also possibly reversible. The peak potential of the reduction of Fe^{3+} to Fe on the CV was observed at about -0.73 V, and the reduction product, Fe, was found to alloy with the Pt electrode. The diffusion coefficient of ferric ions was derived in satisfactory consistency from the CV, SWV, CP, reversal CP, and the CA analyses, and also matched reasonably well with those values in related literature. It was found that there was another reduction reaction with potentials more negative than -1.2 V in CPs. It was considered that the reduction reaction was most likely due to the reduction of Fe^{2+} ions from FeO.

However, it still needs further investigation and confirmation. The transport of O^{2-} ions in the YSZ membrane seemed to have no or little effect on the behavior of electroactive species on the Pt WE in the three-electrode cell at a sufficiently high temperature. Overall, this work has demonstrated the feasibility of electrochemical investigation of ferric ions in molten salts with the aid of the integrated cell with the "O^{2-}| YSZ | Pt | O_2 (air)" RE. We also hope that this work could provide a universal potential reference for the study of other electroactive oxides dissolved in molten salts. It should be noted that the integrated cell as reported in this work is not studied for direct industrial adaption, but the working principle, *i.e.*, using the YSZ membrane for incorporation of RE and also separation of the anode and cathode should be applicable in a future continuous electrolytic steelmaking process, such as the MOE method proposed by Sadoway and co-workers.

REFERENCES

[1] Y. Castrillejo, A. M. Martinez, M. Vega and P. S. Batanero: *J. Appl. Electrochem.*, 1996, vol. 26, pp. 1279-85.

[2] A. Lugovskoy, M. Zinigrad, D. Aurbach and Z. Unger: *Electrochim. Acta*, 2009, vol. 54, pp. 1904-08.

[3] G. M. Haarberga and M. Keppertb: *Ecs. Trans.*, 2009, vol. 16, pp. 309-15.

[4] S. Licht and H. Wu: *J. Phys. Chem. C.*, 2011, vol. 115, pp. 25138-47.

[5] H. Yin, D. Tang, H. Zhu, Y. Zhang and D. Wang: *Electrochem. Commun.*, 2011, vol. 13, pp. 1521-24.

[6] C. Donath, E. Neacsu and N. Ene: *Rev. Roum. Chim.*, 2011, vol. 56, pp. 763-69.

[7] G. M. Haarberg, E. Kvalheim, S. Rolseth, T. Murakami, S. Pietrzyk and S. Wang: *Ecs. Trans.*, 2007, vol. 3, pp. 341-45.

[8] L. Li, X. Liu and S. Wang: in *Energy Technology 2014: Carbon Dioxide Management and Other Technologies*, Eds.: C Wang, J Bakker, C. K. Belt, A. Jha, N. R. Neelameggham, S. Pati, L. H. Prentice, G. Tranell and K. S. Brinkman, John Wiley & Sons, Inc. 2014, pp. 135-40.

[9] S. L. Wang, G. M. Haarberg and E. Kvalheim: *J. Iron Steel. Res. Int.*, 2008, vol. 15, pp. 48-51.

[10] M. A. Quader, S. Ahmed, S. Z. Dawal and Y. Nukman: *Renew. Sust. Energ. Rev.*, 2016, vol. 55, pp. 537-49.

775 [11] S. Jahanshahi, J. G. Mathieson and H. Reimink: *J. Sustain. Metall.*, 2016, vol. 2, pp. 185-90.

776 [12] A. Allanore, L. Yin and D. R. Sadoway: *Nature*, 2013, vol. 497, pp. 353-56.

777 [13] D. H. Wang, A. J. Gmitter and D. R. Sadoway: *J. Electrochem. Soc.*, 2011, vol. 158, pp.
778 E51-54.

779 [14] A. H. C. Sirk, D. R. Sadoway and L. Sibille: *Ecs. Trans.*, 2010, vol. 28, pp. 367-73.

780 [15] A. Allanore: *Electrochim. Acta*, 2013, vol. 110, pp. 587-592.

781 [16] A. Allanore: *J. Electrochem. Soc.*, 2015, vol. 162, pp. E13-E22.

782 [17] G. Z. Chen, D. J. Fray and T. W. Farthing: *Nature*, 2000, vol. 407, pp. 361-64.

783 [18] H. Gao, X. Jin, S. Zou, F. Ling, J. Peng, Z. Wang and G. Z. Chen: *Electrochim. Acta*, 2013,
784 vol. 107, pp. 261-68.

785 [19] G. Li, D. Wang and Z. Chen: *J. Mater. Sci. Technol.*, 2009, vol. 25, pp. 767-71.

786 [20] D. Tang, H. Yin, W. Xiao, H. Zhu, X. Mao and D. Wang: *J. Electroanal. Chem.*, 2013, vol.
787 689, pp. 109-16.

788 [21] A. Cox and D. J. Fray: *J. Appl. Electrochem.*, 2008, vol. 38, pp. 1401-07.

789 [22] Y. Berghoute, A. Salmi and F. Lantelme: *J. Electroanal. Chem.*, 1994, vol. 365, pp. 171-77.

790 [23] K. K. Kasem and S. Jones: *Platinum Metals Rev.*, 2008, vol. 52, pp. 100-06.

791 [24] D. J. Fray: *Metall. Mat. Trans. B*, 2003, vol. 34, pp. 589-94.

792 [25] M.J.U.T. Van Wijngaarden, R. J. Dippenaar and P. M. Van Den Heever: *J. S. Afr. Inst. Min.*
793 *Metall.*, 1987, vol. 87, pp. 269-78.

794 [26] Y. M. Gao, J. X. Song, Y. Q. Zhang and X. M. Guo: *Acta Metall. Sin.*, 2010, vol. 46, pp.
795 277-81.

796 [27] R. Ganesan, T. Gnanasekaran and R. S. Srinivasa: *J. Nucl. Mater.*, 2006, vol. 349, pp. 133-49.

797 [28] T. Ogura, R. Fujiwara, R. Mochizuki, Y. Kawamoto, T. Oishi and M. Iwase: *Metall. Trans. B*,
798 1992, vol. 23B, pp. 459-66.

799 [29] E.T. Turkdogan: *Ironmaking Steelmaking*, 2000, vol. 27, pp. 32-36.

800 [30] P. Soral, U. Pal, H. R. Larson and B. Schroeder: *Metall. Mat. Trans. B*, 1999, vol. 30B, pp.
801 307-21.

802 [31] W. Kim, D. J. Min, Y. S. Lee and J. H. Park: *ISIJ Int.*, 2009, vol. 49, pp. 1882-88.

803 [32] X. Guan, S. Su，U. B. Pal and A. C. Powell: *Metall. Mat. Trans. B*, 2014, vol. 45B, pp.
804 2138-44.

805 [33] A. Krishnan, X.G. Lu and U.B. Pal: *Metall. Mat. Trans. B*, 2005, vol. 36B, pp. 463-73.

806 [34] E. S. Gratz, X. Guan, J. D. Milshtein, U. B. Pal and A. C. Powell, *Metall. Mat. Trans. B*,
807 2014, 45B, pp. 1325-36.

808 [35] Y. M Gao, C. Duan, Y. B. Yang, D. Ruan, C. H. Yang and C. Hong: *ISIJ Int.*, 2015, vol. 55,
809 pp. 2273-82.

810 [36] Y. M. Gao, B. Wang, S. B. Wang and S. Peng: *Journal of Mining and Metallurgy, Section B:*
811 *Metallurgy*, 2013, vol. 49, pp. 49-55.

812 [37] C. Mallika, O. M. Sreedharan and R. Subasri: *J. Eur. Ceram. Soc.*, 2000, vol. 20, pp.

813 2297-2313.

814 [38] S. C. Britten and U. B. Pal: *Metall. Mater. Trans. B*, 2000, vol. 31B, pp. 733-53.

815 [39] C. Z. Wang: *Solid Electrolyte and Chemical Sensors*, Metallurgical Industry Press, Beijing,
816   2000.

817 [40] N. Otsuka: *ECS Transactions*, 2012, vol. 41, pp. 13-19.

818 [41] S. H. Cho, D. Y. Kim, S. Kwon, B. H. Yoon and J. H. Lee: *J. Nucl. Sci. Technol.*, 2018, vol.
819   55, pp.97-103.

820 [42] S.H. Cho, S.W. Kim, D.Y. Kim, J.H. Lee and J.M. Hur: *J. Nucl. Mater.*, 2017, vol. 490,
821   pp.85-93.

822 [43] Y. Gao, C. Yang, C. Zhang, Q. Qin and G. Z. Chen: *Phys. Chem. Chem. Phys.*, 2017, vol. 19,
823   pp. 15876-90.

824 [44] Y. Gao, C. Hong and C. Yang: *J. Electrochem. Soc.*, 2015, vol. 162, pp. E362-69.

825 [45] K. Igarashi, H. Ohtani and J. Mochinaga: *Z. Für Naturforsch. A*, 1987, vol. 42A, pp.
826   1421-24.

827 [46] X. Y. Chen: *Solubility of oxides in molten salts and the preparation of carbide-derived*
828   *carbon by fused salt electrolysis process* (Master's Thesis), Northeastern University,
829   Shenyang, 2012.

830 [47] G. M. Haarberg, E. Kvalheim and S. Rolseth: Electrochemical behaviour of dissolved iron
831   species in molten salts, in *Molten Salts XIV - Proceedings of the International Symposium*,
832   R.A. Mantz et al, Editors, PV 2004-24, The Electrochemical Society Proceedings Series,
833   Pennington, NJ, 2004, p. 890.

834 [48] Factsage 7.1 (Centre for Research in Computational Thermochemistry (CRCT) and
835   GTT-Technologies, 2017), http://www.factsage.com/. Accessed 2 August 2017.

836 [49] J. Yu, W. Yi, B. Chen and H. Chen: *Binary Alloy Phase Diagrams*, Shanghai Scientific and
837   Technical Publishers, Shanghai, 1987, pp. 371.

838 [50] H. E. Ghallali, H. Groult, A. Barhoun, K. Draoui and D. Krulic: *Electrochim. Acta*, 2009, vol.
839   54, pp. 3152-60.

840 [51] A. J. Bard and L. R. Faulkner: *Electrochemical Methods Fundamentals and Applications*,
841   2nd Ed., John Wiley & Sons, Inc, New York, 2001, pp. 226-61.

842 [52] A. J. Bard and L.R. Faulkner: *Electrochemical Methods Fundamentals and Applications*, 2nd
843   Ed., John Wiley & Sons, Inc, New York, 2001, pp. 669-76.

844 [53] H. Tang and B. Pesic: *Electrochim. Acta*, 2014, vol. 119, pp. 120-30.

845 [54] M. Gibilaro, L. Massot, P. Chamelot, L. Cassayre and P. Taxil: *Electrochim. Acta*, 2013, vol.
846   95, pp. 185-91.

847 [55] M. Jayakumar, K. A. Venkatesan and T. G. Srinivasan: *Electrochim. Acta*. 2008, vol. 53, pp.
848   2794-2801.

849 [56] T. Sakurada, H. Maekawa and T. Yokokawa: *Mater. Trans.*, 2007, vol. 39, pp. 740-46.

850 [57] Q. R. Shi, S. Z. Duan and S. M. Wu: *J. Univ. Sci. Technol. B.*, 1994, vol. 16, pp. 599-603.

851 [58] W. Huang, L. Tian, C. She, F. Jiang, H. Zheng, W. Li, G. Wu, D. Long and Q. Li:
852   *Electrochim. Acta*, 2014, vol. 147, pp. 114-20.

853 [59] Z. Chen, Y. J. Li and S. J. Li: *J. Alloys Compd.*, 2011, vol. 509, pp. 5958-61.

854 [60] C. Nourry, P. Souček, L. Massot, R. Malmbeck, P. Chamelot and J.-P. Glatz: *J. Nucl. Mater.*,
855   2012, vol. 430, pp. 58-63.

856 [61] F. H. Hu: *Molten Salt Physical Chemistry*, China Industry Press, Beijing, 1963, pp.73-96.

857 [62] D. Shuzhen, P. Dudley and D. Inman: *J. Electroanal. Chem. Interf. Electrochem.*, 1982, vol.
858   142, pp. 215-28.

859 [63] B. Khalaghia, E. Kvalheima, M. Tokushigeb, L. Teng, S. Seetharamanc and G. M. Haarbergd:
860   *ECS Trans.*, 2014, vol. 64, pp. 301-10.

861 [64] Z. Guangwen, L. Yupin and Z. Yuankai: *Journal of Beijing iron and steel institute*, 1983, (2):
862   68-78.

863 [65] L. Massot, P. Chamelot and F. Bouyer: *Electrochim. Acta*, 2002, vol. 47, pp. 1949-57.

864 [66] S. Frangini and S. Scaccia: *J. Electrochem. Soc.*, 2005, vol.152, pp. A2155-58.

865 [67] V. A. Volkovich, T. R. Griffiths, D. J. Fray and R. C. Thied: *J. Nucl. Mater.*, 2000, vol. 282,
866   pp. 152-58.

867 [68] M. Hayyan, M. A. Hashim and I. M. AlNashef: *Chem. Rev.*, 2016, vol. 116, pp. 3029-85.

868 [69] P. G. Zambonin: *J. Phys. Chem.*, 1974, vol. 78, pp. 1294-98.

869 [70] M. Chandra, S. Vandarkuzhali, S. Ghosh, N. Gogoi, P. Venkatesh, G. Seenivasan, B. P.
870   Reddy and K. Nagarajan: *Electrochim. Acta*, 2011, vol. 58, pp. 150-56.

871 [71] C. Hamel, P. Chamelot and P. Taxil: *Electrochim. Acta*, 2004, vol. 49, pp. 4467-76.

872 [72] A. Wiedenroth and C. Rüssel: *J. Non-Cryst. Solids*, 2004, vol. 347, pp. 180-86.

873 [73] A. Wiedenroth and C. Rüssel: *J. Non-Cryst. Solids*, 2001, vol. 290, pp. 41-48.

874 [74] E. Freude: *Voltammetrische Untersuchung des Redoxverhaltens polyvalenter Ionen in*
875   *Glasschmelzen*, insbesondere von Technetium,Thesis Erlangen, 1989.

876 [75] C. Rüssel and E. Freude: *Glastech. Ber.*, 1990, vol. 63, pp. 149-53.

877 [76] O. Claussen and C. Rüssel: *Glastech. Ber. Glass Sci. Technol.*, 1996, vol. 69, pp. 95-100.

878 [77] A.W.M. Wondergem·de Best: *Redox behaviour and fining of molten glass* (Doctoral Thesis),
879   Technische Universiteit Eindhoven, 1994, pp. 126

880 [78] K. Serrano and P. Taxil: *J. Appl. Electrochem.*, 1999, vol. 29, pp. 505-10.

881 [79] A. J. Bard and L. R. Faulkner: *Electrochemical Methods Fundamentals and Applications*,
882   2nd Ed., John Wiley & Sons, Inc, New York, 2001, pp. 161-65.

883 [80] J. De Strycker, P. Westbroek and E. Temmerman: *J. Electroanal. Chem.*, 2004, vol. 565,
884   pp.149-58.

885 [81] Y. M. Kan, S. L. Li, P. L. Wang, G. J. Zhang, O. V. de Biest and J. Vleugels: *Solid State*
886   *Ionics*, 2008, vol. 179, pp. 1531-1534.

887 [82] Z. G. Lv, P. Yao, R. S. Guo and F.Y. Dai: *Mat. Sci. Eng. A*, 2007, vol. 458, pp. 355-360.

888

Tables：

Table I. Transition Time Data from Fig. 4(a).

I (mA)	τ_{red} (s)	τ_{ox} (s)	τ_{red}/τ_{ox}
±10	—*	1.63	—
±11	7.40	1.41	5.2
±12	5.13	1.17	4.4
±13	4.00	1.10	3.6
±14	3.05	1.04	2.9

I applied current, τ_{red} Reduction transition time, τ_{ox} xidation transition time.

* The exact value cannot be obtained.

Table II. Collections for Diffusion Coefficients of Ferric Ions in Similar Molten Halide Salts.

Salt composition (Weight Percent)	Fe$_2$O$_3$ (Weight Percent)	WE/RE	MT	$D\times10^5$ (cm^{2}s^{-1})	T (K)	Refs.
65CaCl$_2$-35NaCl	0.5	Pt/YSZ|Pt|O$_2$(air)	CV	4.9±0.5[†]	1273	This work
				1.8±0.1[‡]		
			SWV	6.7±0.4[†]		
				2.4±0.1[‡]		
			CP	7.5±0.6		
			Reversal CP	7.5±0.7		
			CA	4.8±0.2		
CaCl$_2$-NaCl*	0.28	Mo/Ag	CV	9.4±0.7	1123	6
85CaCl$_2$-15CaF$_2$	0.6	Mo/Pt	CV	3**	1100	7
79CaCl$_2$-9.7CaF$_2$-11.3KF	0.4	Mo/Fe	CV	5.3	1100	8
89.1CaCl$_2$-10.9KF	0.4	Mo/Fe	CV	9.7	1100	8
90CaCl$_2$-10KF	0.6	Mo/Pt	CV	9.7	1100	9

WE/RE, working electrode/reference electrode; MT, measurement technique; CV, cyclic voltammetry; SWV, square wave voltammetry; CP, chronopotentiometry; CA, chronoamperometry.

* The proportion of CaCl$_2$ and NaCl is not found in the paper.

** The calculation process is unknown from the paper.

[†]Passing through the origin.

893

894

895

896   **Figure Captions：**

897

898   Fig. 1—Schematic illustration of the YSZ-based integrated three-electrode cell for
899   electrochemical analyses in molten salt at high temperatures (1273 K in this work).

900

901   Fig. 2—A typical OCP-time plot recorded in the course of immersing the Pt wire WE into the
902   molten mixture containing 0.5 wt pct Fe_2O_3 and then switching from Ar to air in the furnace tube
903   (*a*); a typical WE potential-time curve recorded in the polarization experiment (*b*), and a typical
904   AC impedance Nyquist plot recorded at the OCP (bias potential) (*c*). RE: O^{2-} | YSZ | Pt | O_2 (air).

905

906   Fig. 3—CVs recorded in molten $CaCl_2$-NaCl at 1273 K with 0.5 wt pct Fe_2O_3 at *v* (potential scan
907   rate) = 0.04, 0.05, 0.06, 0.07, 0.08, 0.10, 0.50, or 1.00 V s^{-1}, and without Fe_2O_3 (blank) at *v* = 50
908   mV s^{-1} (*a*), and correlations of I_{pc} (reduction peak current) and E_{pc} (reduction peak potential) with
909    $v^{1/2}$ (*b*). RE: O^{2-} | YSZ | Pt | O_2 (air).

910

911   Fig. 4—Reversal CPs on the Pt WE in molten $CaCl_2$-NaCl with 0.5 wt pct Fe_2O_3 at 1273 K and
912   different currents (±10, ±11, ±12, ±13 and ±14 mA) (*a*) and the correlation of the $I\tau^{1/2}$ (τ:
913   transition time) value against the cathodic current *I* for the reduction plateau (*b*). RE: O^{2-}| YSZ | Pt
914 | O_2 (air).

915

916   Fig. 5—LSVs recorded at 50 mV s^{-1} on the Pt wire WE under the static and rotating modes after
917   the potentiostatic electrolysis for 30, 60, 90 seconds in molten $CaCl_2$-NaCl with 0.5 wt pct Fe_2O_3.
918   Inset: a set of typical current-time curves of potentiostatic electrolysis using the Pt wire WE for 30,
919   60, 90 seconds. Potentiostatic electrolysis potential: -0.76 V; time: 30, 60, 90 s; temperature: 1273
920   K; RE: O^{2-}| YSZ | Pt | O_2 (air).

921

922   Fig. 6—SEM image of the cross section of the Pt wire WE (*a*), EDS analyses of spots 1 and 2 in
923   the SEM image (*b*), and the line scanning profiles of Pt (*c*), Fe (*d*) and O (*e*) after potentiostatic
924   electrolysis in molten $CaCl_2$-NaCl with 0.5 wt pct Fe_2O_3. Potentiostatic electrolysis potential: -
925   0.73 V; time: 30 min; temperature: 1273 K; RE: O^{2-} | YSZ | Pt | O_2 (air).

926

927   Fig. 7—XRD pattern for the Pt foil WE after potentiostatic electrolysis in molten $CaCl_2$-NaCl
928   with 0.5 wt pct Fe_2O_3. Potentiostatic electrolysis potential: - 0.7 V; time: 30 min; temperature:

929   1273 K; RE: O^{2-} | YSZ | Pt | O_2 (air).

930

931   Fig. 8—SWVs recorded in the molten $CaCl_2$-NaCl mixture with 0.5 wt pct Fe_2O_3 at different

932   frequencies (30, 40, 50, 60, 70, 80 Hz) and 1273 K (*a*) and the correlations between the peak

933   current (I_p), the peak potential (E_p), and the square root of the frequency ($f^{1/2}$) , respectively (*b*).

934   RE: O^{2-} | YSZ | Pt | O_2 (air).

935

936   Fig. 9—CPs recorded in the melt with 0.5 wt pct Fe_2O_3 at 1273 K at different cathodic currents of

937   -8, -10, -11, -12, -13, -14, -14 mA (*a*) and the correlation between the cathodic current I and the

938    $I\tau^{1/2}$ (τ: transition time) value for the reduction plateau (*b*). RE: O^{2-} |YSZ | Pt | O_2 (air).

939

940   Fig. 10—CAs recorded in the melt with 0.5 wt pct Fe_2O_3 at 1273 K at different step potentials of

941   -0.5, -0.6, -0.7, -0.8, -0.9, -1.0, -1.1, -1.2 V (*a*) and the correlation between the cathodic current I

942   and the $t^{-1/2}$ value at different step potentials of -0.8, -0.9, -1.0, -1.1, -1.2 V (*b*). RE: O^{2-} |YSZ | Pt |

943   O_2 (air).